UncorrelaTEd

Solid-liquid thermoelectric systems with uncorrelated properties

Deliverable 1.2: Phenomena that influence the power factor improvements in the Sb:SnO$_2$ systems

Project partners

LOGO	Partner full name	Acronym
	Universitat Jaume I	UJI
	Institut de Recerca en Energia de Catalunya	IREC
	Kungliga Tekniska Högskolan	KTH
	University of Warwick	UW
	Solvionic	SOLV
	Specific Polymers	SP

Deliverable Name: Phenomena that influence the power factor improvements in the Sb:SnO$_2$ systems

Led by: UJI

Partners: UJI, SOLV, IREC

Version	Date	Changes
1.0	30/07/2021	Original version

Index

Figure index

Table index

1 Introduction

This derivable reports on the identification of the phenomena that produce the power factor (*PF*) improvements identified in preliminary results for the Sb:SnO$_2$ (ATO) films. Understanding the reasons behind these improvements will be key to move the strategies employed in Sb:SnO$_2$ to the other materials of the project (Bi-Te alloys, oxides and polymers), which will have thermoelectric (TE) properties close to the state of the art.

2 Objectives

The main objective of WP1 is the identification of the phenomena that produce the *PF* improvements already observed in Sb:SnO$_2$ devices. To achieve this objective, up to 4 different tasks were planned. In Task 1.1, porous films produced from commercial Sb:SnO$_2$ nanoparticles with different porosity levels were fabricated, in order to evaluate the influence of porosity in the *PF* improvements. Details of the fabrication of these films can be found in the D1.1.

The rest of the tasks of WP1 are devoted to identify the phenomena responsible for the *PF* improvements in 3 different types of electrolytes: inert (Task 1.2) and electroactive (Task 1.3) salts dissolved in solvents, and ionic liquids (Task 1.4). The results obtained in Tasks 2 to 4 is what is covered in this deliverable. Within the Results section, one subsection will be devoted to each type of electrolyte.

All these tasks are necessary to fulfil the objective 1: Identify in detail the processes, already observed in the hybrid solid-liquid TE system with the Sb:SnO$_2$ solid material of modest TE properties, that resulted in breaking the adverse *S-σ* interdependence.

3 Results

3.1 Inert salts

This subsection focuses on identifying the reasons behind the improvements in the *PF* found in the preliminary results of Table 1. These preliminary results were obtained by the UJI group before the beginning of the project. It should be mentioned that both HI and LiI are not actually inert salts, since I$^-$ can exchange electrons with the electrodes and the ATO material. At the beginning of the project we thought that this would not be the case.

Table 1. Seebeck coefficient, device electric resistance, and PF enhancement values of Sb:SnO$_2$ films with and without the presence of different electrolytes.

Electrolyte	Seebeck coefficient (µV/K)		Electric resistance (kΩ)		$\dfrac{PF_{with}}{PF_{without}}$
	Without electrolyte	*With electrolyte*	*Without electrolyte*	*With electrolyte*	
1 M LiI in H$_2$O	-35.8	-53.6	9.5	1.3	**16.4**
1 M HI in H$_2$O	-37.9	-212.8	19.3	17.0	**35.8**

3.1.1 Sb:SnO$_2$ film fabrication and characterisation

Unless otherwise mentioned, the ATO films employed in this study were prepared by spin coating by UJI. They were fabricated using microscope slide glasses (1 mm thickness) cut (25 mm x 15 mm size) and cleaned by three steps of sonication during 15 min. In the first step, using a soap/water solution (1:10 v/v). Then, in distilled water to remove soap excess, and finally, in isopropanol. After this, substrates were dried under compressed air flow and treated in a UV Ozone cleaner (Ossila, L2002A2-UK) for 20 min. Subsequently, an Sb:SnO$_2$ colloidal aqueous dispersion (Keeling and Walker, ref. A20W) was deposited by spin coating (Laurell, WS-650MZ-23NPPB) at 2500 rpm for 15 s. Five layers were deposited. After each deposition, a drying process was carried out on a hot plate at 100 ºC for 10 min. Later on, an annealing was performed at 550°C for 45 min in a furnace (Nabertherm, 400-1) with a 3 °C/min heating rate. For the electric contacts at each side of the film, in some cases a thin chromium layer (5 nm) was deposited at 25 nm/min rate by sputtering (Quorum Technologies, Q300 TD plus) followed by the deposition on top of it of a platinum layer at 8 nm/min rate during 12 min. In other cases, Ag paint (RS, ref. 1239911) was employed, which was left to cure for at least overnight before its use.

The morphological characterisation by SEM and TEM (Fig. 1) reveals that the film is formed by nanoparticles with size range among 6 and 10 nm (Fig. 1c and d). The film thickness was estimated around 1 µm (Fig. 1b), whereas the chromium-platinum contact films were ≈100 nm.
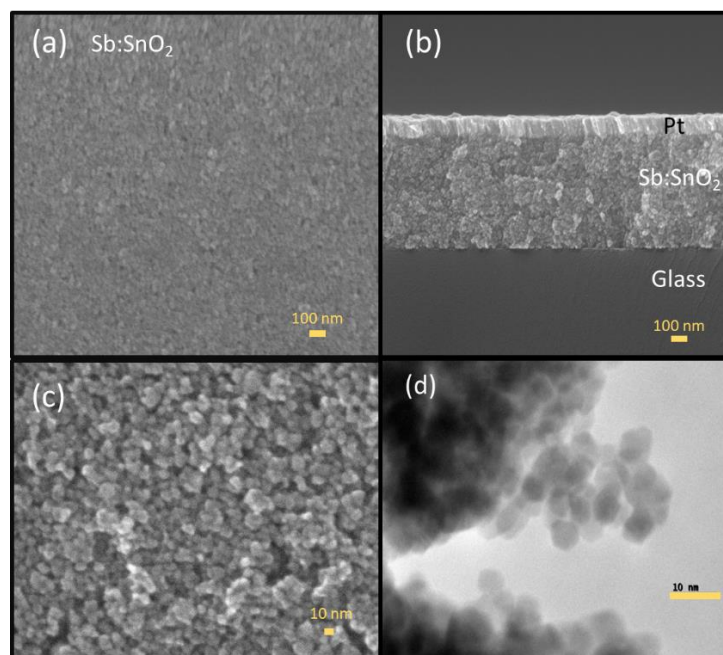
Fig. 1. (a, b, c) SEM and (d) TEM images of an Sb:SnO$_2$ film. (a, c) Top views at different magnifications, (b) a cross-sectional view of a region with the Cr/Pt contact deposited.

The film composition was analysed by energy disperse X-ray (EDX) analysis, where the emission peaks were correlated with chemical elements (Fig. 2). The analysis showed that the ATO film was doped with 10 % of antimony.

Element	Weight%	Atomic%	Compd%	Formula
Sn L	71.38	30.61	90.63	SnO_2
Sb L	7.83	3.27	9.37	Sb_2O_3
O	20.79	66.12		
Totals	100.00			
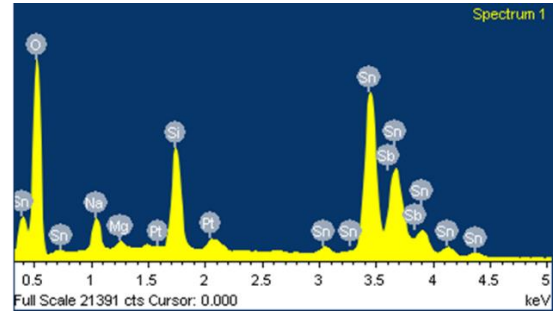
Fig. 2. Energy disperse X-ray elemental analysis of Sb:SnO₂ (ATO) film.

The structure of the film was analysed by X-ray diffraction (seeFig. 3). The characteristic peaks match with the cassiterite phase (SnO_2) according to the powder pattern reference R040017. The presence of antimony could not be observed in the diffractogram (no shift in the peaks).
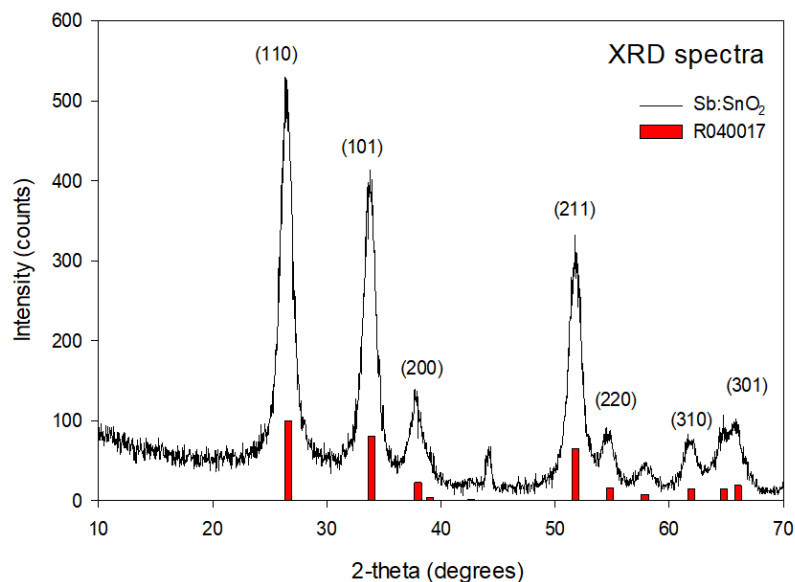
Fig. 3. X-ray diffraction diffractogram of Sb:SnO₂.

3.1.2 TE properties measuring setup

The TE measurements were carried out in a homemade setup (Fig. 4), which consist of copper blocks with inserted cartridge heaters as the heat source at the hot side, and a large copper block at the cold side acting as heat sink (Fig. 4a). The glass substrate with the film deposited was placed on top of the copper blocks and a PTFE bridge. The latter helps to avoid breaking the sample during the time a pressure is applied (Fig. 4a). Thermal grease (RS, ref. 2173835) was used to improve the substrate/copper thermal contacts. A holed polytetrafluoroethylene (PTFE) block with a squared O-ring at the bottom was placed on top of the glass substrate to allow the location of the electrolyte (Fig. 4b). The PTFE block also has holes for positioning two thermocouples and several screws to provide a gentle pressure for sealing the central rectangular hole and avoid electrolyte leakage. Two thermocouples (K-type, RS, ref. 8140134) were placed on top of the glass substrate through the PTFE holes with a bit of thermal grease at their tips for thermalisation (Fig. 4c). The electric contacts were made with two spring probes at the edges of the film.

The resistance of the device was measured by current-voltage (I-V) curves using a Source Meter (Keithley 2450) under no temperature difference (values under 5 K temperature difference were similar). A delay time of 1 ms was used for each current value applied. The Seebeck coefficient values were obtained from the slope of the open-circuit voltage (V_{oc}) vs the temperature difference (ΔT) plot. The ΔT is the difference between the temperature at the hot side and the cold side, which was varied from 0 to 5 K. The voltage was registered by a nanovoltmeter (Keithley 2182A), and the thermocouples were connected to a dual thermometer (RS, ref. 1316). All the measurements were performed using shielded cables and inside a Faraday cage.
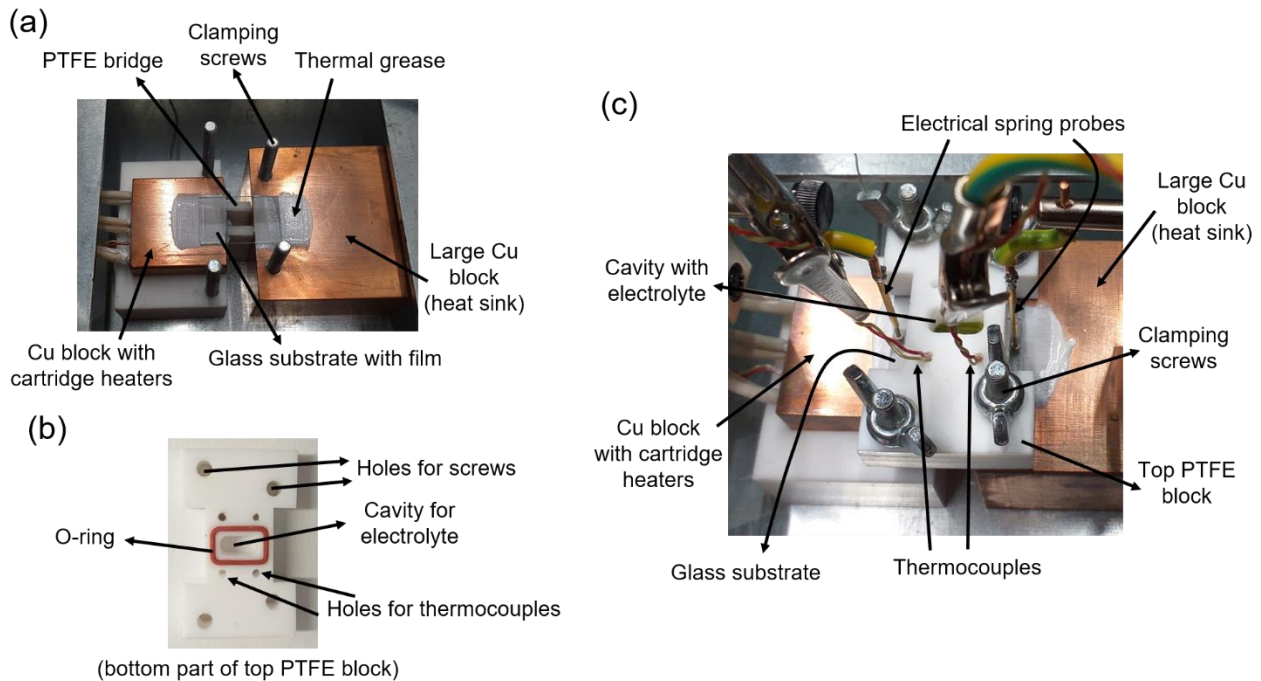
Fig. 4. Pictures of the thermoelectric characterisation setup. (a) Setup with the top PTFE block not assembled. (b) Bottom part of the top PTFE block. (c) Complete setup assembled.

3.1.3   Contacts corrosion evaluation

Both LiI and HI electrolytes are corrosive, which can cause degradation in the metallic contacts of the device. To ensure that contact degradation will not be present in the devices, we tested gold and platinum contacts, both with a thin chromium seeding layer underneath to improve the contact adherence with glass. In both metallic contacts deposited on a glass substrate (without ATO), we added drops of 1M HI and 1M LiI aqueous electrolytes (see Fig. 5). Visual inspections were performed in both metallic contacts after different times (2 and 36 h). After two hours, some degradation could be observed in the gold film, while platinum was stable (see Fig. 5). At 36 h, the gold degradation became more notorious and platinum remained stable. Consequently Cr/Pt contacts were selected for the devices to be studied.
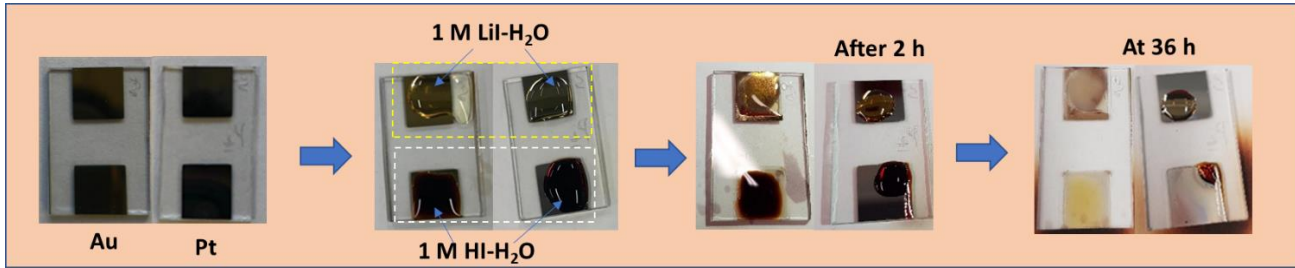
Fig. 5. Gold and platinum contacts pictures before and after entering into contact with the electrolytes at different times.

3.1.4   Thermoelectric characterization results

The Seebeck coefficient (*S*) and device resistance (*R*) results for the Sb:SnO$_2$/1M HI in H$_2$O system are shown in Table 2. Seebeck coefficient and electric resistance were measured for three similar samples (S5, S19, S20) without and with electrolyte. After the addition of the electrolyte, the Seebeck coefficient increased in all cases and the resistance dropped significantly, reaching similar values to those found in our preliminary results (Table 1). However, although S19 and S20 showed similar results, a significant difference was found for sample S5, which exhibited a much lower Seebeck coefficient improvement.

Table 2. Thermoelectric properties identified in different samples of the ATO/HI system.

Electrolyte: 1M HI in H$_2$O	Seebeck coefficient (µV/K)		Electric resistance (kΩ)	
	Without electrolyte	*With electrolyte*	*Without electrolyte*	*With electrolyte*
Sample S5	-65.20	-86.09	5.53	0.89
Sample S19	-50.42	-216.96	3.86	0.21
Sample S20	-47.77	-203.83	2.68	0.22

The results of the Sb:SnO$_2$/1M LiI in H$_2$O system are presented in Table 3 for three similar samples (S4, S6, S19). A similar trend to that observed in the previous system with the HI electrolyte was found. Two samples (S6 and S9) showed a significant improvement in *S*, while a lower improvement occurred for S4. All cases showed a significant device resistance reduction.

Table 3. Thermoelectric properties identified in different samples of the ATO/LiI system.

Electrolyte: 1M LiI in H$_2$O	Seebeck coefficient (µV/K)		Electric resistance (kΩ)	
	Without electrolyte	*With electrolyte*	*Without electrolyte*	*With electrolyte*
Sample S4	-65.10	-86.48	18.29	3.67
Sample S6	-55.69	-162.77	4.83	0.28
Sample S19	-59.51	-164.53	8.46	0.46

We realised after the measurements in some of the LiI systems that the electrolyte showed a change of colour from transparent to dark brown. This was due to the reaction shown in Fig. 6, which leads to the presence of I$_3^-$ (brown). So, the observed results in both systems (Table 2 and Table 3) could be due to the presence of a redox couple (I$^-$/I$_3^-$). To validate this assumption, a fresh electrolyte was prepared, consisting of 1 M LiI and 10

mM I_2, which is equivalent to the I^-/I_3^- couple. Using this electrolyte, we tested different samples (see Table 4, samples S14-S17). A huge increment in the Seebeck coefficient values was observed, while the electric resistance dropped due to the presence of the electrolyte, which corroborate that the redox couple (I^-/I_3^-) is responsible for the improvements observed in all the systems.

(a)   (b)
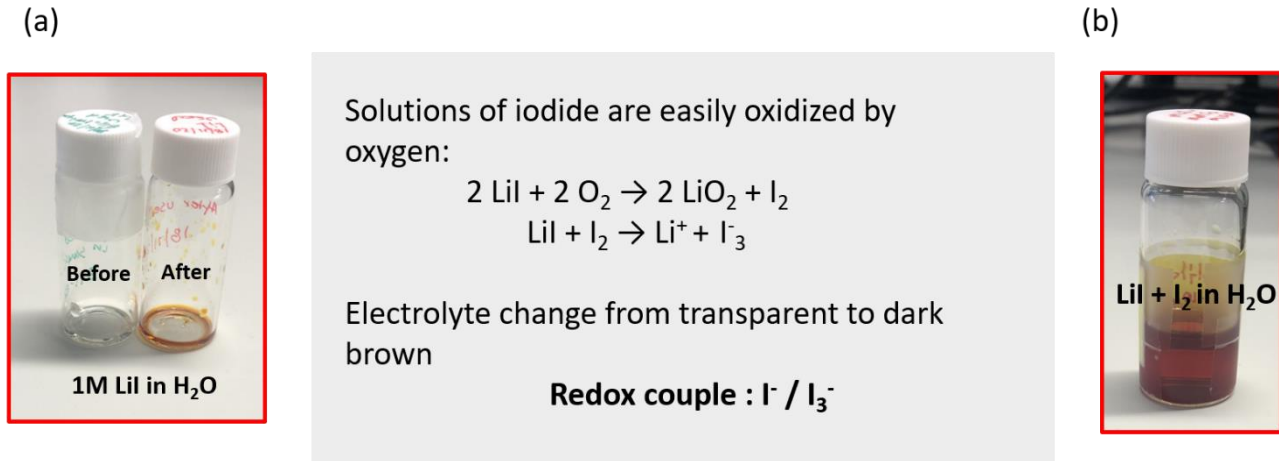
Fig. 6. (a) LiI electrolyte before and after the thermoelectric measurements. (b) Electrolyte with LiI and I_2, which from the I^-/I_3^- redox couple, as indicated by the chemical reactions in the centre of the figure.

Apart from these results, Table 4 also shows the measurements in a device with the same configuration but without the ATO film, that is, two Pt contacts separated by the electrolyte, which is the configuration of a thermocell.[1] As it can be observed in Table 4, the sample with no ATO (thermocell) showed a Seebeck coefficient value close to those found when ATO is present. Moreover, the device resistance is nearly the same than that obtained for all the ATO samples. This is an evidence that ATO is doing nothing in the hybrid devices, and the results observed when the electrolyte is present are due to a thermocell configuration, i.e., the current flows through the electrolyte and the Seebeck coefficient is governed by the electrolyte.

Table 4. Thermoelectric properties identified in different samples of the ATO/LiI+I_2 system (S14-S17) and for a sample where ATO is not present (Pt/electrolyte/Pt).

Electrolyte: 1M LiI + 10 mM I_2	Seebeck coefficient (µV/K)		Electric resistance (kΩ)	
	Without electrolyte	*With electrolyte*	*Without electrolyte*	*With electrolyte*
Sample S14	-64.04	-435.90	5.45	0.11
Sample S15	-65.09	-365.09	6.02	0.12
Sample S16	-77.04	-468.87	6.34	0.09
Sample S17	-95.49	-572.35	4.03	0.11
No ATO		-370.43		0.11

This is an unfortunate and completely unexpected result, since those electrolytes were identified as the most promising for the project. However, we were able to identify an alternative strategy that led to results even better. This new strategy is reported in section 3.2.2.

3.2 Electroactive salts

In this subsection, hybrid devices using ATO as TE material were put into contact with electroactive salts (which can exchange electrons with the metallic electrodes and ATO) dissolved in solvents. The initially targeted electroactive molecule was chromium (III) acetylacetonate, which was dissolved in 3-methoxypropionitrile (3-MPN), a high boiling point organic solvent. Apart from this electrolyte, the ferro/ferricyanide complexes [$K_4Fe(CN)_6$ / $K_3Fe(CN)_6$] dissolved in water were also studied.

3.2.1 Chromium (III) acetylacetonate

The electrolyte prepared for this study, 0.1 M Cr (III) acetylacetonate dissolved in 3-MPN, does not have the corrosion problems of the previous electrolytes, and Ag paint (RS, ref. 1239911) contacts were used, since they showed better reproducibility than Pt contacts.

In Table 5, it is shown the variation of the Seebeck coefficient and the device resistance without and with the presence of the electrolyte for 3 similar samples of ATO with Ag paint contacts. It can be observed that the absolute value of the Seebeck coefficient experiences an average drop of 22.7%, while the device resistance also reduces an average value of 59.4%. This leads to an average *PF* improvement of 1.51 times.

Table 5. Seebeck coefficient, device electric resistance, and PF enhancement values of Sb:SnO₂ films with and without the presence of 0.1 M Cr($C_5H_7O_2$) in 3-MPN.

Sample	Seebeck coefficient (µV/K)		Device electric resistance (kΩ)		$\dfrac{PF_{with}}{PF_{without}}$
	Without electrolyte	With electrolyte	Without electrolyte	With electrolyte	
S1	-55.7	-40.1	12.7	3.89	**1.71**
S2	-57.3	-42.3	18.5	7.56	**1.34**
S3	-59.4	-51.2	10.2	5.08	**1.48**

In order to evaluate if the observed decrease in the device resistance is due to electronic conduction through the electrolyte, a sample formed by only the Ag paint contacts and the electrolyte (no ATO) was tested. This sample showed no clear trend of the open-circuit voltage with the temperature difference (no Seebeck response) and its resistance was 4.58 MΩ, which is two orders of magnitude above the resistance of the samples without electrolyte of Table 5. Thus, electronic conduction through the electrolyte can be discarded and is not behind the observed resistance reduction.

In order to clarify further the role of the Cr($C_5H_7O_2$) complex, we also evaluated 3 samples with an electrolyte with no Cr complex, i. e. ATO contacted by Ag paint contacts and permeated by only 3-MPN. Results are shown in Table 6. It can be observed that the absolute value of the Seebeck coefficient drops in this case an average value of 29.5%, similar to the case of the system with the Cr complex in the electrolyte. However, the device resistance, although also reduces, it only experiences an average 38.2% drop, which is far from the 59.4% drop of the Cr complex system. The observed variations lead to an average *PF* decrease of 0.84 times. This clearly indicates that the Cr complex is necessary in the electrolyte to produce the *PF* improvements.

Table 6. Seebeck coefficient, device electric resistance, and PF enhancement values of Sb:SnO₂ films with and without the presence of 3-MPN (no Cr(C₅H₇O₂).

Sample	Seebeck coefficient (µV/K)		Device electric resistance (kΩ)		$\dfrac{PF_{with}}{PF_{without}}$
	Without electrolyte	With electrolyte	Without electrolyte	With electrolyte	
S4	-57.7	-36.9	16.5	9.4	**0.72**
S5	-57.1	-43.1	8.7	5.4	**1.00**
S6	-49.1	-35.5	13.4	8.9	**0.80**

Since the electrical conduction takes place through the ATO film, the variation in the device resistance should be due to a change in the electrical conductivity of ATO. The electrical conductivity of a material σ depends on the carrier density n, and the carrier mobility μ, since $\sigma=qn\mu$, being q the elementary charge (q=1.6x10⁻¹⁹ C). The mobility of the carriers is not expected to change in the system, since the structure of the film does not vary, hence, we attribute the reduction of the resistance to an increase in the carrier concentration, which can be achieved by the injection of electrons from the Cr complex into the ATO when the oxide equilibrates with the electrolyte. The variation observed in the system with no Cr complex (Table 6), can be due to the equilibration with residual water molecules, which are present in the 3-MPN. A variation in the electrical conductivity is typically accompanied by a reduction in the absolute value of the Seebeck coefficient, which was also observed experimentally (see Table 5).

3.2.2   Ferro/ferri-cyanide

In order to find promising results after identifying in section 3.1 that the best *PF* improvements were due to the presence of a thermocell (ATO was doing nothing), we decided to try another approach, consisting in achieving the Seebeck coefficient of an electrolyte (e.g. 1.43 mV/K of the ferro/ferricyanide compounds in water in a thermocell)[1] in an electrically conducting material (metal) without affecting its electrical conductivity.

In a thermocell, two metals (usually Pt) are separated by a redox couple electrolyte. The metals (electrodes) equilibrate their energy level with the energy level at the electrolyte when brought into contact. If a temperature difference appears, the entropy of the redox species changes and so the energy level in the electrolyte, which could move the level in the metal, giving rise to *S* values in the order of mV/K. In our new approach, we considered that the same process could occur if a continuous piece of metal is in contact with the electrolyte, rather than two metals separated by the electrolyte, but with the benefit in this case that current will flow through the metal.

In order to validate this new approach, we tested 3 different samples using the setup of Fig. 4: (i) a sample with two very thin (<8 nm) Pt contacts separated (thermocell configuration), (ii) a continuous very thin (<8 nm) Pt layer, and (iii) ATO film with Pt contacts that will not enter into contact with the electrolyte. These samples are shown in Fig. 7a, which also indicates the area that will be in contact with the electrolyte by the red dashed lines. Fig. 7b shows the schematic of the measuring setup for the case of the continuous Pt film.
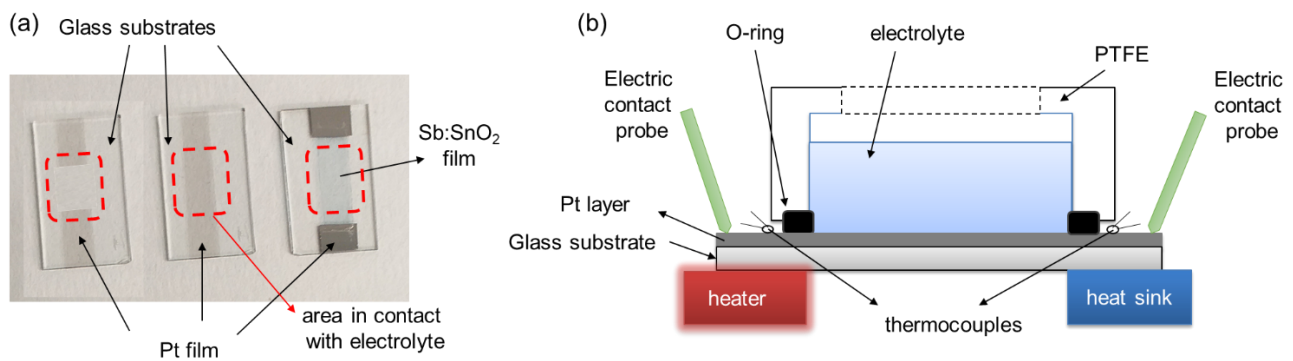
Fig. 7. (a) Pictures of the different samples prepared in this task and (b) the schematic of the measuring system for the case of a continuous Pt film.

The 3 different samples of Fig. 7a were brought into contact with a 0.4 M ferro/ferri-cyanide redox couple dissolved in milli-Q water, and the TE properties were determined before and after the contact with the electrolyte (see Table 7). The sample with the thermocell configuration (separated Pt contacts) showed the expected *S* value (1.848 mV/K) and a similar value (1.473 mV/K) was found for the continuous film sample, hugely different from the value of the film without the electrolyte (1.71 µV/K). In addition, the resistance remained similar to the value without electrolyte, even slightly reduced (see Table 7). This remarkable result demonstrates that our approach works, and the Seebeck coefficient of a redox electrolyte can be transferred to Pt without affecting its electrical conductivity.

The sample with ATO showed a similar result to that found in the continuous Pt film, and the Seebeck coefficient of the sample in the presence of electrolyte achieved a value of 2.349 mV/K, even higher than the value of the thermocell configuration (see Table 7). Moreover, the electric resistance of the device significantly dropped from 34 to 9.6 kΩ. This proves that the approach also works in an oxide (semiconductor), so it could probably be applied to any electrically conducting material.

Table 7. Thermoelectric properties identified in different devices of the ferro/ferri-cyanide system.

Sample	Seebeck coefficient (µV/K)		Electric resistance (kΩ)	
	Without electrolyte	*With electrolyte*	*Without electrolyte*	*With electrolyte*
Separated Pt contacts	-	1,848	-	18.1
Continuous Pt film	1.71	1,473	9.9	7.8
Pt/ATO/Pt	-90.4	2,349	34.0	9.6

In the case of the continuous Pt film, the thickness plays a crucial role, as shown in Fig. 8. In this figure, continuous films of different thickness were evaluated, and, as it can be observed, the *S* value achieved when the samples are in contact with the same ferro/ferri-cyanide electrolyte significantly decreases when the thickness is increased. This possibly occurs due to the fact that the electrons in the material affected by the presence of the electrolyte are only those close to the surface, so large surface area to film volume ratios are needed for this approach to work. In fact, this is fulfilled in the sample with ATO (see Table 7), where due to

the nanostructured morphology that creates a large surface area, the strategy works in the film, which is around 1 μm thick.
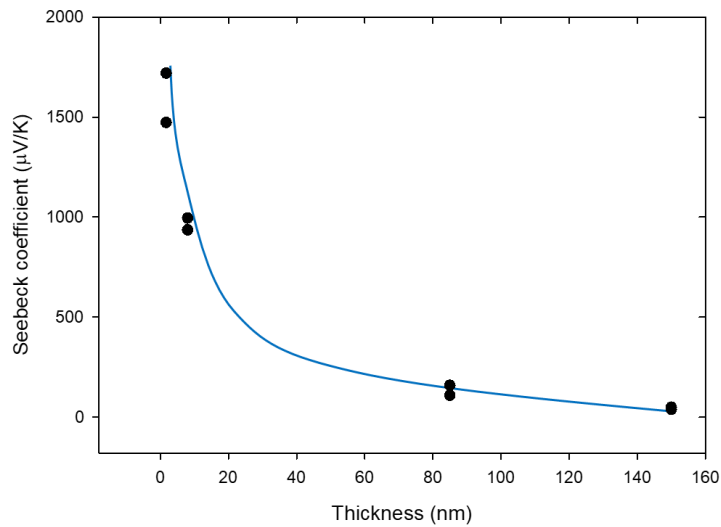
Fig. 8. Variation of the Seebeck coefficient of continuous Pt films of different thickness in contact with a ferro/ferri-cyanide electrolyte.

This new approach has an enormous potential and could lead to unprecedented efficiencies in the heat-to-electricity energy conversion by TE materials, which can even be cheap and abundant. This potential is shown in Fig. 9, which represents ZT values of different families of materials vs price at 300 K, considering that they can adopt a *S*=1.4 mV/K, which is the typical value of the ferro/ferri-cyanide electrolyte.[1] It should be mentioned that corrections will be required for the thermal conductivity, since the contribution to the thermal conduction from the electrolyte is not included. However, large changes are not expected, since liquids typically have low thermal conductivity values [0.1-0.6 W/(Km)]. As it can be observed in the figure, unprecedented values above 20 or even above 200 can be potentially achieved, being the most attractive materials in terms of performance the metal foams, which are ideal for this new UncorrelaTEd approach due to their high surface area to volume ratio. In addition, cheap alloys such as steels, magnesium, aluminium and zinc could provide large ZTs at a very low price.

Work on developing further this new strategy will continue in the project. In addition, UJI has submitted a patent application for its future exploitation.
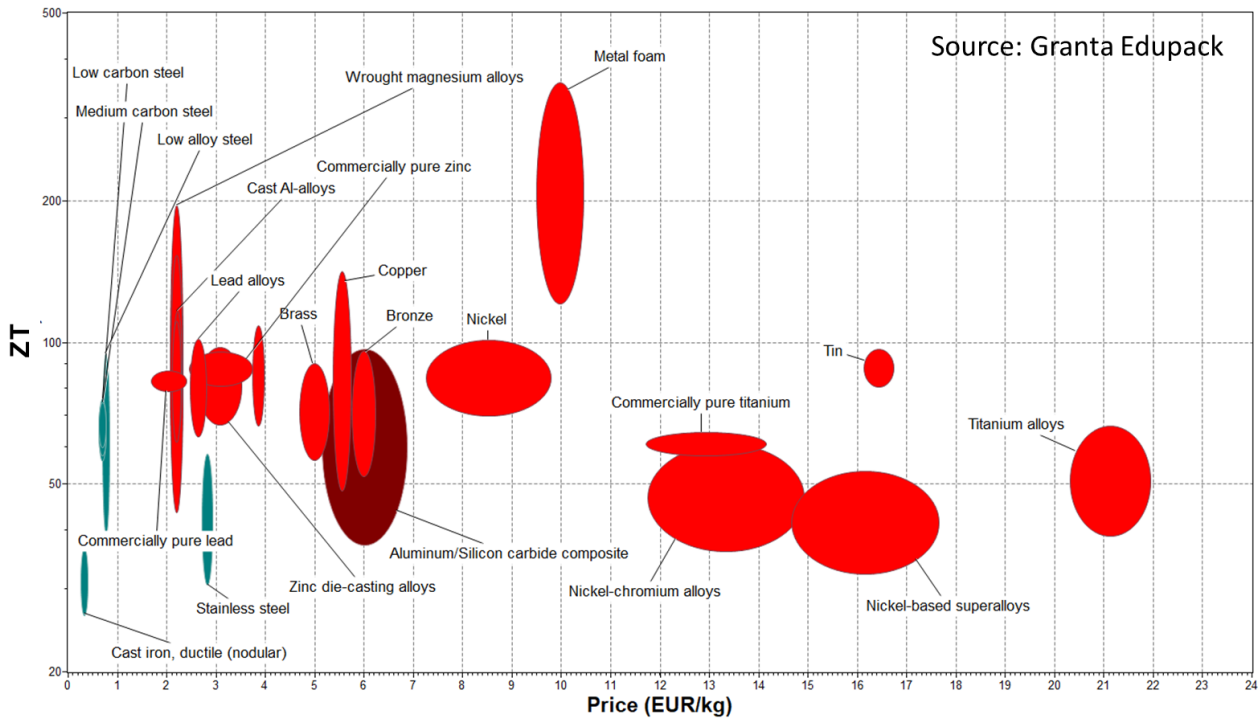
Fig. 9. Potential ZTs of different families of materials calculated at 300 K and assuming they can exhibit a Seebeck coefficient of 1.4 mV/K.

3.3 Ionic liquids

SOLV prepared different ionic liquids in order to understand the processes behind the *PF* improvements observed in these systems in a previously published paper by UJI with ATO as TE material.[2] SOLV synthesised five different imidazolium-based ionic liquids to be used as electrolytes (see Fig. 10). Imidazolium-based salts are indeed liquid at room temperature.

Comparable ionic liquids of the type XMImI (X=Hexyl, Propyl, Butyl; MIm=methylimidazolium) were fabricated in order to evaluate the influence of the size of the cation and more particularly the cation chain-length. On the other end, three combinations of ionic liquids BMImY (Y=I, BF_4, TFSI) were chosen to study the influence of the anion.

Fig. 10. Imidazolium-based ionic liquids to study the influence of cation chain-length and nature of anions.

It should be noted that in this study we employed sealed cells, fabricated as described in our previous work,[2] instead of using the setup of Fig. 4. We also used Ag paint for the metallic contacts at the ends of the ATO film. A picture of one of the sealed cells can be seen in Table 8. In this table, it can be also observed the variation of the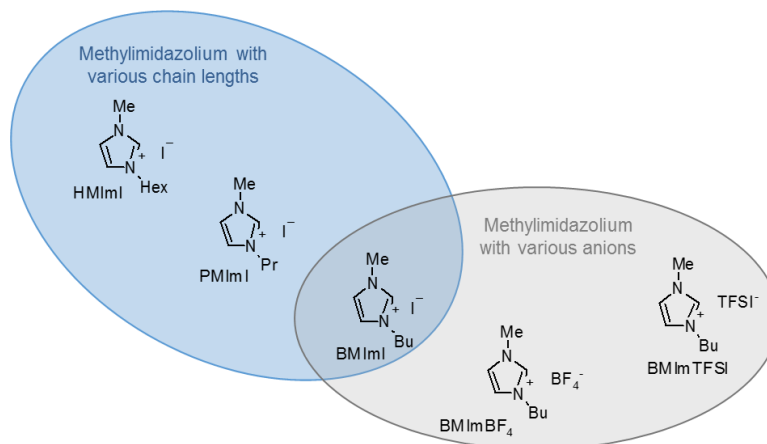 Seebeck coefficient and the device resistance without and with the presence of the BMImI ionic liquid as electrolyte (cell Ag-ATO/BMImI-Ag). This system was already tested in our previous work, where an average 35.0% reduction in the absolute value of the Seebeck coefficient and an 82.5% decrease in the device resistance was found.[2] In Table 8, it can be observed that the absolute value of S decreases 37.8%, and the device resistance drops 90.4%, which are values close to the ones previously reported. These variations lead to a *PF* improvement of 4.05 times.

In order to evaluate if the significant drop in the device resistance could occur due to electrical conduction through the electrolyte, a cell with only the ionic liquid in contact with the Ag contacts (no ATO) was tested (cell Ag-BMImI-Ag in Table 8), which is a configuration similar to a thermocell. In this case, no clear trend of the open-circuit voltage was observed when the temperature difference was changed, so S could not be provided. On the other hand, due to the slow response of the system, the *I-V* curve was obtained under steady-state condition, that is, different voltage values were applied and their corresponding current values were recorded when the steady state was reached (after ≈600 s). The resistance value identified (42.32 kΩ) is in the same order of magnitude that the value of the cell without electrolyte (23.0 kΩ). This makes possible the conduction through the electrolyte, thus, we investigated this possibility further.

Table 8. Seebeck coefficient, device electric resistance, and PF enhancement values of different cells using BMImI as electrolyte.

Cell	Seebeck coefficient (µV/K)		Device electric resistance (kΩ)		$\dfrac{PF_{with}}{PF_{without}}$
	Without electrolyte	With electrolyte	Without electrolyte	With electrolyte	
Ag-ATO/BMImI-Ag	-66.36	-41.27	23.0	2.20	**4.05**
Ag-BMImI-Ag	-	-	-	42.32	**-**

For the analysis of this issue, we performed electrochemical impedance spectroscopy experiments in the three different configurations of Table 8: (i) only the ATO contacted by Ag (Ag-ATO-Ag), (ii) the ATO in contact with BMImI (Ag-ATO/BMImI-Ag) and (iii) the cell with only the electrolyte and no ATO (Ag-BMImI-Ag). The impedance experiments are shown in Fig. 11a. They were performed under no temperature difference at 0 V dc and using an amplitude of 1 mV in the frequency range 10 mHz – 1 MHz for Ag-ATO-Ag and 5 mHz – 1 MHz for the other two configurations, which might show a slower response time.

It can be seen from Fig. 11a that the response of the Ag-ATO-Ag cell consists of a semicircle, whose last points (dc or steady state limit) reach a value of the real part of the impedance of 23.0 kΩ, in agreement with the resistance value of Table 8. We attribute the semicircle to the parallel combination of a resistance with a capacitance, related to the large amount of boundaries existing between neighbouring nanoparticles in the film.[3] The response from the Ag-BMImI-Ag cell consists of a semicircle as well, which was quite noisy around the middle frequencies. Several points have been removed from the spectrum for this reason. It should be

noted that apart from the semicircle a straight line of around 45º slope appears at low frequencies (right side). This response can be due to a charge transfer between the Ag electrodes and the I⁻ anions (semicircle) which is controlled by the ions diffusion (straight line) at low frequencies, which is the response reported for thermocells.[4] The Ag-ATO/BMImI-Ag cell shows a semicircle similar to the one observed for the Ag-ATO-Ag cell, and no ionic diffusion (45º straight line) is present (see inset of Fig. 11a). The lack of the straight line indicates that conduction through the electrolyte is not taking place, and the system has basically become more conducting when BMImI is present due to an increase in the electrical conductivity of ATO.
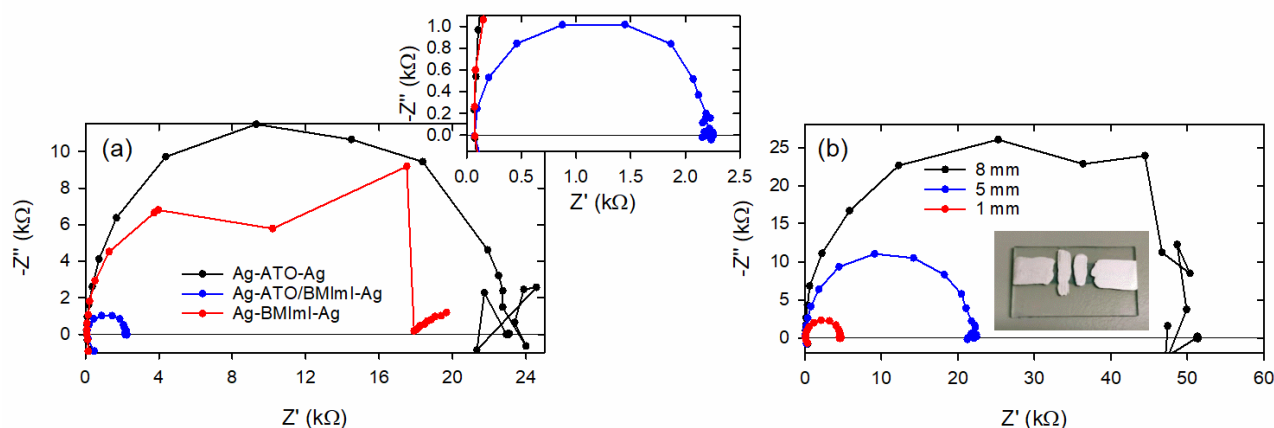

Fig. 11. Impedance spectra of (a) different cells of the system with BMImI electrolyte and (b) the ATO film at different distances from the left contact. Inset in (a) is magnification of the bottom left part. Inset in (b) is a picture of the film with Ag paint strips at the different distances.

To further support this conclusion, we measured the impedance response of an ATO film contacted by Ag paint contacts at several distances, which were achieved by painting Ag strips onto the film at different positions (see inset of Fig. 11b). The impedance response was measured first between the left and right-side Ag contacts (with no Ag strips present), which are separated a distance of ≈8 mm. The response obtained for this sample (Fig. 11b) is similar to that of the Ag-ATO-Ag cell (Fig. 11a), as expected. After performing this measurement, a Ag strip separated ≈5 mm from the left contact was painted on the film and left to cure overnight. The impedance response was then measured. After this, another strip was painted at a distance of ≈1 mm repeating the process. It can be observed in Fig. 11b that reduced semicircles were obtained according to the reduction in the distance, supporting that a reduction of the ATO resistance leads to a reduction of the semicircle, as observed in the Ag-ATO/BMImI-Ag system (Fig. 11a).

We attribute the reduction of the resistance to the same mechanism suggested for the Cr complex in section 3.2.1. The variation of the electrical conductivity of ATO can be obtained by an increase in the carrier concentration, which can be achieved by the injection of electrons from the I⁻ ions when the ATO equilibrates with the electrolyte. As occurred for the Cr complex electrolyte, the variation of the electrical conductivity is also accompanied here by a reduction in the absolute value of the Seebeck coefficient (see Table 8).

We have focused only in the BMImI ionic liquid in this deliverable since the studies using the other ionic liquids was still in progress at the time of the preparation of this deliverable, and hence not yet completed. Consequently, this deliverable will be updated in the coming months once the studies pending are completed.

3.4 Evaluation of the effect of the ATO film porosity

During WP1 it was planned to analyse the effect of the ATO film porosity on the *PF* improvements, since surface level interactions takes place in the systems and an increase of the surface exposed to the electrolytes might have a crucial effect. For that purpose, IREC prepared ATO films of different porosity (see D1.1 Procedure to fabricate $Sb:SnO_2$ films of different porosity). When these films were tested at UJI, after being in contact with the different electrolytes under study, unexpectedly, significant parts of the films seemed to collapse and became powder, losing the consistency of the films (see Fig. 12). A further annealing of the films was tried to see if that could improve the films consistency but it did not work. This issue made not possible to conduct the planned study of the influence of porosity unfortunately. However, since solid materials with different porosity levels will be prepared in WP2 (bismuth telluride alloys) and WP3 (ZnO and $Ca_3Co_4O_9$) the effect of porosity will be analysed using these films in the corresponding WPs.
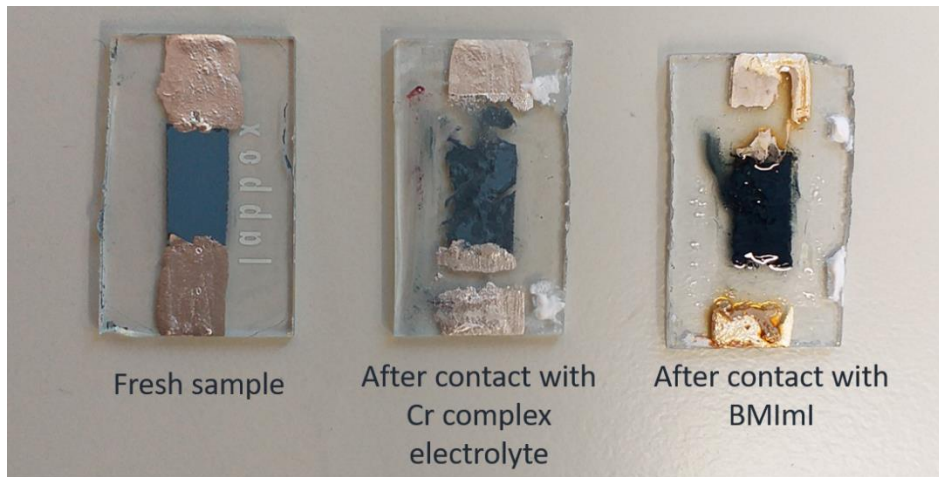

Fig. 12. Degradation experienced by ATO films prepared by IREC after being in contact with the Cr acetylacetonate electrolyte and the BMImI ionic liquid.

4 Conclusions

The main objective of this deliverable is to report the identification of the phenomena that produce the power factor improvements already observed in preliminary studies with $Sb:SnO_2$ devices. This connects with the 1st objective of the project: Identify in detail the processes, already observed in the hybrid solid-liquid thermoelectric system with the $Sb:SnO_2$ solid material of modest thermoelectric properties, that resulted in breaking the adverse *S-σ* interdependence.

Three different systems were analysed for this purpose. In all of them, nanostructured $Sb:SnO_2$ was used as the solid material, and the electrolyte varied. First, 1M HI and 1M LiI aqueous electrolytes were analysed. These electrolytes produced 35.8 and 16.4 times improvements in the power factor, respectively, in the preliminary results. Similar results were obtained here in our analysis, which were due to a huge increase in the absolute value of the Seebeck coefficient, that reached values close to -160 and -200 µV/K, accompanied by a significant drop in the device resistance of an order of magnitude. We realised that in these electrolytes a reaction with O_2 dissolved in the solution can produce I_3^- and, hence, the I^-/I_3^- redox couple can be present

in the electrolyte. A device with only this redox couple (no Sb:SnO$_2$), which is the configuration of a thermocell, was tested, and showed Seebeck coefficient and device resistance values close to those found when Sb:SnO$_2$ is present. Thus, it was found that Sb:SnO$_2$ is doing nothing in these systems and the large power factor improvements observed when the electrolyte is present are due to the existence of a thermocell configuration (current flows through the electrolyte and the Seebeck coefficient is also governed by the electrolyte).

The 2nd type of electrolyte analysed was formed by electroactive species dissolved in a solvent. A chromium (III) acetylacetonate complex dissolved in 3-methoxypropionitrile (0.1 M concentration) was first studied. For this electrolyte, the absolute value of the Seebeck coefficient experienced an average drop of 22.7%, while the device resistance was reduced an average value of 59.4%, which turned into an average power factor improvement of 1.51 times. Different experiments discarded the possibility that electrical conduction through the electrolyte exists, and proved that when the Cr complex is not present in the electrolyte (in a cell with only the 3-methoxypropionitrile), no power factor improvements were produced. The variation observed in the properties of this system can be explained by the increase of the electrical conductivity of Sb:SnO$_2$, due to an increase in their carrier concentration, which can be achieved by the injection of electrons from the Cr complex. The variation in the electrical conductivity is typically accompanied by a reduction in the absolute value of the Seebeck coefficient, which also occurred.

Using also electroactive species, we tried another approach in order to reach power factor improvements at least larger than those from the preliminary results (35.8 times). This approach consists in achieving the Seebeck coefficient of an electrolyte (e.g. 1.43 mV/K of the ferro/ferricyanide compounds in water in a thermocell) in an electrically conducting material (e.g. a metal) without affecting its electrical conductivity. Using Pt as the conducting material the approach was demonstrated, leading to unprecedented improvements in the power factor. It was identified that the approach is strongly affected by the thickness of the films, being more beneficial large surface area to volume ratios. Also, a nanostructured porous film, such as the ATO prepared in this work, is demonstrated to be suitable to apply this approach. This strategy has been patented by the UJI group and will be explored further in the project, since it can lead to dimensionless figure of merits *ZT*s above 20.

The third type of electrolytes analysed was formed by ionic liquids. In our previously reported article,[2] an average 35.0% reduction in the absolute value of the Seebeck coefficient and an 82.5% decrease in the device resistance was found for BMImI. Our analysis of this system, performed using electrochemical impedance measurements, led to the conclusion that the resistance reduction was due to the same mechanism suggested for the Cr complex, i.e. the electrical conductivity of ATO was increased by increasing the carrier concentration, which can be achieved by the injection of electrons from the I$^-$ ions when the ATO equilibrates with the electrolyte. This variation of the electrical conductivity was also accompanied by a reduction in the absolute value of the Seebeck coefficient.

Finally, although investigating the effect of porosity in the power factor improvements was planned, it was not possible, since the ATO films prepared by IREC lost their consistency during the measurements with the electrolytes. However, the influence of this parameter will be investigated in WP2 (with bismuth telluride) and WP3 (with ZnO and Ca$_3$Co$_4$O$_9$).

5 References

1. Dupont, M. F., MacFarlane, D. R. & Pringle, J. M. Thermo-electrochemical cells for waste heat harvesting-progress and perspectives. *Chem. Commun.* **53**, 6288–6302 (2017).

2. Márquez-García, L., Beltrán-Pitarch, B., Powell, D., Min, G. & García-Cañadas, J. Large Power Factor Improvement in a Novel Solid–Liquid Thermoelectric Hybrid Device. *ACS Appl. Energy Mater.* **1**, 254–259 (2018).

3. Irvine, J. T. S., Sinclair, D. C. & West, A. R. Electroceramics: Characterization by Impedance Spectroscopy. *Adv. Mater.* **2**, 132–138 (1990).

4. Yang, P. & Fan, H. Electrochemical Impedance Analysis of Thermogalvanic Cells. *Chem. Res. Chinese Univ.* **36**, 420–424 (2020).